PNAS RESEARCH ARTICLE | CELL BIOLOGY

Mining cancer genomes for copy number alterations identifies glycosylation enzymes as oncogenic drivers

Pranoy Sahu[a,1], Francesco Russo[a,1], Domenico Russo[a], Ilenia Agliarulo[a], Pasqualina Ambrosio[a], Riccardo Rizzo[b], Matteo Lo Monte[a], Nicola Normanno[c], Silvia Soddu[d], Francesca Carlomagno[a,e], Alberto Luini[a,2], and Seetharaman Parashuraman[a,2]

Affiliations are included on p. 10.

Edited by Chi-Huey Wong, The Scripps Research Institute, La Jolla, CA; received August 9, 2025; accepted January 22, 2026

Altered cell-surface glycans are established cancer biomarkers, yet no oncogenes have been identified within glycan biosynthesis machinery. This represents a critical gap, as defining a gene as a true oncogene, rather than merely a component of an oncogenic pathway, reveals targetable dependencies that can improve clinical decisions. To date, no gain-of-function mutations have been detected in glycogenes, and the search for such mutations is largely saturated. To address this gap, we developed a bioinformatic–experimental pipeline to identify copy number alteration (CNA)-based driver genes, overcoming noise from passenger genes. The approach recovered known oncogenes and tumor suppressors, while revealing novel candidates, including glyco-oncogenes. Focusing on the glycosphingolipid (GSL) biosynthetic pathway, we validated *B4GALT5* as a bona fide glyco-oncogene whose genomic amplification drives proliferation, oncogene addiction, and poor prognosis, effects that can be reversed by targeted pathway inhibition. Mechanistic studies show that B4GALT5 promotes cancer cell survival via integrin-Src signaling under anchorage-independent conditions. Collectively, these findings establish glycosylation enzymes as a druggable oncogene class and provide a resource of high-confidence CNA-based cancer regulatory genes.

oncogenes | glycosphingolipids | copy-number alterations | golgi

Significance

In this study, we reveal that cancer can be driven by genomic amplification of glycogenes, expanding the repertoire of druggable oncogenes. Using our pipeline, we identified *B4GALT5*, encoding a key enzyme of the glycosphingolipid (GSL) pathway, as an oncogene whose activity enables more precise patient stratification, both by copy number alterations (CNA) in glycosylation genes and by dependencies on downstream regulatory kinases such as c-Src. These findings introduce glycosylation enzymes as a new, targetable class of cancer drivers, opening new opportunities for cancer therapy.

Carcinogenesis leads to changes in the cell-surface glycome, resulting in the display of several glycans that promote cancer (1–3). Since the 1960 s, aberrant glycans have been recognized as cancer biomarkers (4, 5), and accumulating evidence shows that glycan alterations are not only highly frequent but also contribute to cancer initiation, progression, and immune evasion. However, it is not sufficient for a gene to be "overexpressed" or "tumor-promoting" to make it a cause of tumorigenesis. Gene expression is a fluctuating parameter, influenced by the microenvironment, sample quality, and transient regulatory events. Relying solely on "high levels" for diagnosis creates a gray zone of false positives (tumors that express the gene but are not tumorigenic because of it). By contrast, an oncogene represents a stable alteration in the tumor's DNA. Its identification shifts diagnosis from general statistical correlations to a causal molecular mechanism and provides a much stronger rational justification for therapeutic intervention.

In this study, we sought to determine whether bona fide oncogenes might exist within the glycosylation machinery. To date, no glycogene is listed as a cancer driver in the COSMIC Cancer Gene Census. This absence represents a critical gap in cancer biology: Historically, the identification of genetically defined driver genes has transformed our understanding of tumorigenesis and reshaped diagnostic classification and therapeutic decision-making. The lack of confirmed cancer drivers arising from glycosylation pathways limits our mechanistic insight into how aberrant glycosylation contributes to malignant progression and restricts opportunities to develop targeted therapeutic strategies against this essential biosynthetic network.

The classification of a gene as a bona fide oncogene requires the demonstration of at least three defining features. First, the gene must harbor a recurrent, statistically significant genetic alteration in patient tumors, such as an activating mutation, focal copy-number gain, or oncogenic fusion. Second, this alteration must result in a demonstrable increase in the activity of the encoded gene product. Third, the resulting gain of activity must be functionally linked to cellular transformation, survival, and growth. These criteria establish a causal relationship between a specific genomic alteration and a malignant phenotype, distinguishing true oncogenic drivers from genes whose expression changes merely accompany or facilitate tumor progression. Applying these principles to the glycosylation network allows reassessment of whether glycosylation genes occupy a central, genetically defined role in cancer biology.

Author contributions: P.S., F.R., A.L., and S.P. designed research; P.S., F.R., D.R., I.A., P.A., R.R., and M.L.M. performed research; F.C., A.L., and S.P. contributed new reagents/analytic tools; P.S., F.R., N.N., S.S., F.C., A.L., and S.P. analyzed data; and P.S., F.R., A.L., and S.P. wrote the paper.

Competing interest statement: A.L. is the co-founder of private start-up Golgenia Srl., a startup interested in developing glycan-based cancer therapeutics.

This article is a PNAS Direct Submission.

[1]P.S. and F.R. contributed equally to this work.

[2]To whom correspondence may be addressed. Email: a.luini@ieos.cnr.it or seetharaman.parashuraman@cnr.it.

This article contains supporting information online at https://www.pnas.org/lookup/suppl/doi:10.1073/pnas.2521848123/-/DCSupplemental.

Published April 1, 2026.

The mutational landscape of cancer has been extensively charted over the past decade and is now considered largely saturated for common tumor types (6). Yet this exhaustive effort has not revealed any recurrent, activating point mutations in genes encoding the glycosylation machinery. However, major alternative mechanisms, such as genomic amplification, for generating oncogenes have not been extensively explored despite whole-genome sequencing advancements. Guided by recent technological advancements, focal amplifications have been exploited to identify and validate classical signaling oncogenes, such as receptor tyrosine kinases, cyclins, and transcriptional regulators. Instead, metabolic and glycosylation genes have been comparatively understudied despite their potential as druggable drivers, leaving a vast space for identification of novel oncogenes.

A notable exception is *GOLPH3*. A decade ago, this Golgi-localized protein was shown to acquire oncogenic properties when genomically amplified in human cancers (7). Subsequent studies established that GOLPH3's oncogenic activity depends on two distinct but potentially integrated functions. First, GOLPH3 promotes secretion by facilitating cargo exit from the trans-Golgi network (8). Second, as shown by our group (9) and others (10), GOLPH3 regulates the sorting of specific glycosylation enzymes into COPI-coated vesicles (9–11). Through this mechanism, elevated GOLPH3 levels remodel the composition of cell-surface glycans, particularly glycosphingolipids (GSLs), in ways that enhance cell growth and survival (9). Following GOLPH3, several other Golgi-localized proteins have been identified as oncogenes (12–14), although whether they exert their effects through the regulation of glycosylation remains unclear.

Motivated by the above considerations, we systematically searched for cancer-regulatory genes among glycogenes, focusing on genomic copy number alteration (CNA). We developed a CNA-based prioritization pipeline that identifies candidate oncogenes and tumor suppressor genes within amplified or deleted regions. This approach not only correctly recovered known cancer drivers, validating its robustness but also revealed several previously unappreciated candidates. These include multiple glycosylation enzymes belonging to different glycosylation pathways.

We then focused on genes encoding components of the GSL biosynthetic pathway, which emerged prominently from our analysis, and validated them as potential oncogenic regulators with clinical relevance. Among the seven GSL-associated oncogenes identified, *B4GALT5* serves as an illustrative example. Although *B4GALT5* had been previously implicated in tumor progression, it had never been demonstrated to function as a bona fide oncogene, partly limiting the attention it received in mechanistic and translational studies. Using a combination of genetic, biochemical, and phenotypic assays, we demonstrate that *B4GALT5* fulfills all key criteria of an oncogene and acts through the integrin–Src signaling axis, establishing a direct mechanistic link between GSL biosynthesis, Golgi function, and oncogenic signaling.

Results

Identification of Potential Cancer Regulatory Genes Based on CNA. To identify potential oncogenes/TSGs from among the multiple genes present in the CNA segment, we developed a pipeline based on a method described by Santarius and colleagues (15) (Fig. 1*A*). For this analysis, we used The Cancer Genome Atlas dataset provided by cBioportal (www.cbioportal.org) (16). The dataset consisted of genomic, transcriptomic, and clinical data of 10,845 patients covering 32 cancer types (*SI Appendix*, Table S1). For each cancer type, the copy number data for 24,776 genes were obtained as GISTIC (Genomic Identification of Significant Targets in Cancer) scores (17).

To identify the CNA segments of a chromosome, we focused only on those genes that showed true amplification (copy number > 4) or homodeletion (both copies deleted). The frequency of gene(s) CNA was plotted along the chromosomal length. A background threshold was calculated to identify genes with statistically significant CNA (Fig. 1*A* and *SI Appendix*, *Methods*). Only the CNA segments of length of 1 kb to 100 Mb (19) were considered for further analysis to concentrate on focal CNAs (fCNAs). This resulted in 6,920 copy number altered segments–2,413 amplified and 4,507 deleted—across the cancer types. In 18 cancer types, where published data were available, we identified a median of 76% of the published amplified segments and 64% of the published deleted segments in our study (*SI Appendix*, Fig. S1*B*). The median frequency of patients showing copy number amplifications was 3.3% and those with copy number deletions was 2.2%. Nearly 99% of the identified CNAs were present in less than 15% of the patients in each cancer type (*SI Appendix*, Fig. S1*D*). These numbers in general reflect earlier published frequencies of CNAs in cancer (19).

Next, we identified those genes that also have a statistically significant change in expression levels ($P < 0.05$ in a Wilcoxon–Mann–Whitney test with Benjamini–Hochberg correction) and in the appropriate direction i.e., an increase in case of gene amplifications and a decrease in case of gene deletions. This resulted in the 7,722 Class IV oncogenes and 4,865 Class IV TSGs (see above) being selected across all the cancer types (Fig. 1*B* and *SI Appendix*, Fig. S1*C*).

Prioritization of Potential Cancer Regulatory Genes. Next, to prioritize the Class IV cancer regulatory genes, we analyzed the following characteristics of these genes:

Clinical: 1. Correlation of CNA with patient survival.

Bioinformatic: 2. Sole identified gene in the CNA segment; 3. CNA and mutations are mutually exclusive; 4. Documented evidence for inherited mutation in the gene leading to cancer (based on OMIM); 5. Alteration or mutations of other genes in the same pathway (based on Reactome).

Biological: 6. Overexpression of the gene of interest promotes cell growth in vitro (20) (for amplification); 7. Downregulation of a Class IV gene in a cell line where it has CNA alters cell growth/viability (data from DepMap database); 8. Transposon-mediated deletion/inactivation promotes carcinogenesis in animals (based on candidate cancer gene database; for deletion).

Each of these characteristics was assigned a point and those Class IV genes that acquire 1 or 2 points were classified as Class III cancer regulatory genes and those that get 3 or more points were classified as Class II cancer regulatory genes. Classification as Class I oncogene depends on clinical drug targeting (15) and we did not study this aspect.

We used a Kaplan–Meier analysis to compute univariate survival curves, and a log-ratio test was performed. Only those genes that show CNA in at least five patients were considered for analysis which was done in a cancer-stage matched manner (when data were available). Altogether, based on the points scored we were able to classify 2,493 genes as Class III oncogenes and 39 as Class II oncogenes. As for TSGs, 1,547 were found to be Class III TSGs and 147 were found to be Class II TSGs (Fig. 1*B* and Dataset S1; for more, see https://frusso.shinyapps.io/CNA_database/). The source code of the prioritization pipeline can be found here: https://github.com/franruss/Prioritization-of-driver-genes-based-on-CNA/tree/main.

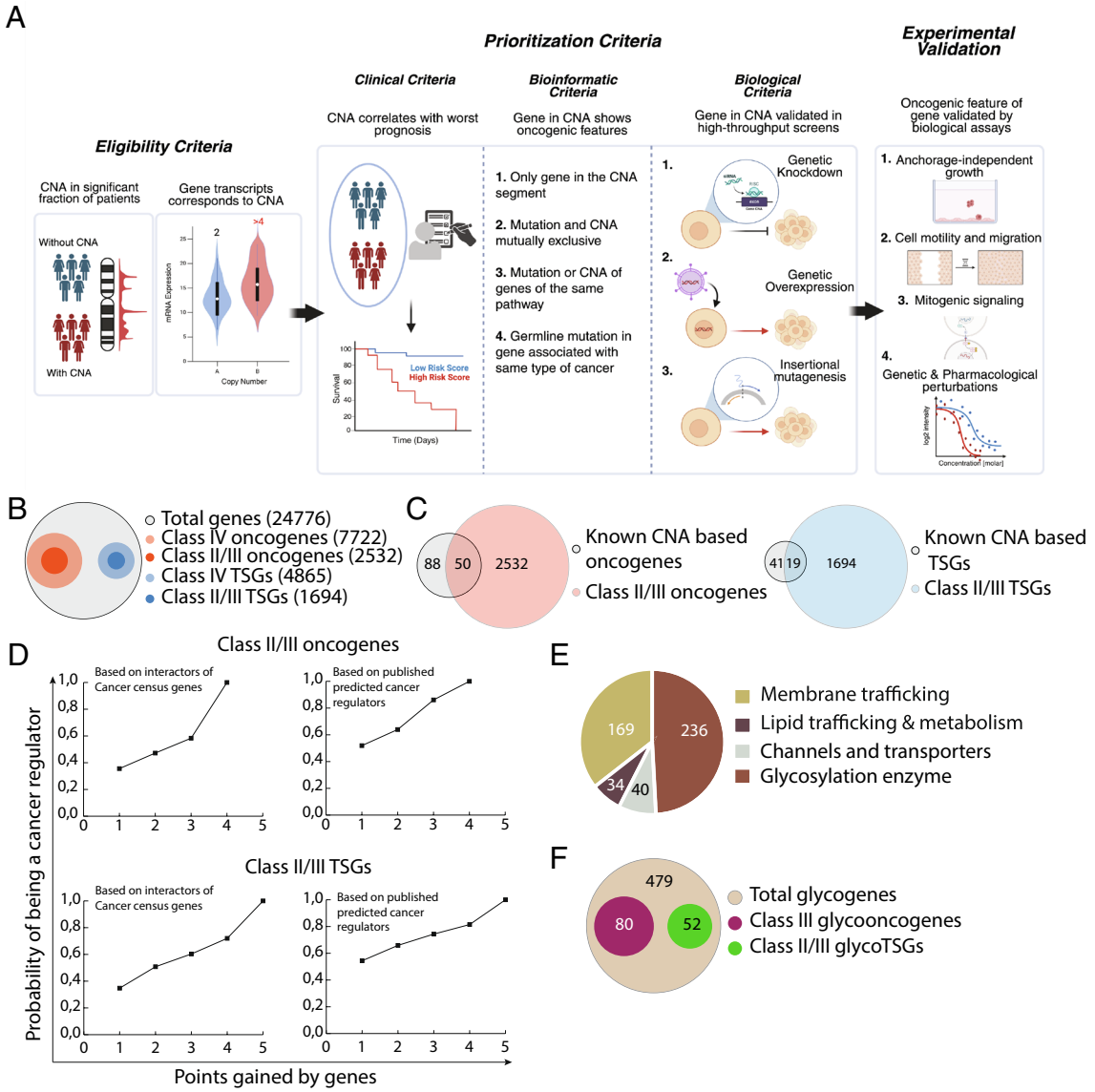

Fig. 1. Pipeline to identify significant cancer regulatory glycogenes based on CNA. (*A*) Pipeline to identify and prioritize genes with significant CNA in the cancer genomes. Made using the Bio Render graphical tool. (*B*) Venn diagrams showing the relationship between total number of genes analyzed and the indicated class of genes that were identified. (*C*) Venn diagrams of the total number of Class II/III cancer regulatory genes identified with respect to the known CNA-based cancer regulatory genes. (*D*) The fraction of prioritized cancer regulatory genes (*Upper* panel: Class II/III oncogenes; *Lower* panel: Class II/III TSGs) of indicated points presented in the list of cancer census genes interactors or predicted oncogenes (18) was analyzed and plotted here as probabilities. (*E*) Classification of glycogenes analyzed in the study. (*F*) Venn diagrams showing the relationship between total number of glycogenes analyzed, the number of identified Class II/III glyco-oncogenes or glyco-TSGs.

Novel Cancer Regulatory Genes. Among the previously identified 88 known amplification-based oncogenes, 50 were identified as Class II/III genes in our analysis while of the 41 known CNA-based tumor suppressors, 19 were identified as Class II/III genes (Fig. 1*C* and Dataset S2). While the prioritized list of genes was enriched in several known cancer regulatory genes, we wanted to know if this list also includes novel cancer regulatory genes. To do this, we compared our list of prioritized oncogenes with two other lists of likely oncogenes. One contained direct interactors of the known oncogenes that are expected to be enriched in novel oncogenic regulators (18) and the other consisted of a list of published potential oncogenes characterized by their similarity to established oncogenes (21).

We downloaded human protein interaction data of the 723 COSMIC cancer census genes from the STRING database (from https://version-11-0.string-db.org) (threshold at 0.4 with experimental interaction only). There were 4.722 interactors of the cancer census genes. Among these interactors, we found 795 of the prioritized oncogenes and 553 of the prioritized TSGs identified by our algorithm. This overlap was statistically significant (Fisher Exact Test; P-value < 10^{-16}) (*SI Appendix*, Fig. S1*E*). Given that the prioritized list of oncogenes is divided into different classes based on points, we sought to analyze if there was a correlation between the points acquired by a gene and the probability that it is present in one of the lists of potential oncogenes that we used. We noted that higher the points acquired by a gene it is more likely to be present in these lists (Fig. 1*D*). Genes with 4 or 5 points had a probability of 1 *i.e.,* they were present in the list. The genes with 1 point had a probability of 0.25. Genes with 3 and 2 points had probabilities of roughly 0.7 and 0.5, respectively. Given that most of the genes had a score of 1 we think at least 1/4th of the oncogenes and TSGs identified in Dataset S2 will be potential true positives.

Based on these probability scores and overlap with the other two datasets of cancer regulatory genes we made a high confidence

list of cancer regulatory genes that were predicted by our method as well as the two other methods mentioned earlier. This resulted in a list of 68 novel high-confidence oncogenes and 143 novel high-confidence TSGs based on CNA (>50% probability; Dataset S3). Given that nearly 10,000 genes or half the genome showed statistically significant CNA this result of about 100 oncogenes/TSGs shows nearly 100-fold enrichment for potential cancer regulatory genes. Thus, we conclude that the prioritized CNA-based oncogene/TSG list is enriched in several novel cancer regulatory genes.

Glyco-Oncogenes and Glyco-TSGs. To identify glycan-based cancer regulatory genes from the list of prioritized cancer regulatory genes, we first built a dataset of 479 glycogenes from literature search and manual curation (Fig. 1*E* and Dataset S4). The genomic distribution of these genes showed no specific chromosomal enrichment (*SI Appendix*, Fig. S1 *F* and *G*). We intersected this list with that of the prioritized cancer regulatory genes and found 80 Class III glyco-oncogenes (of which 28 were glycosylation enzymes) and 52 Class III glyco-TSGs (of which 26 were glycosylation enzymes) (Fig. 1*F*). As a fraction of all Class III cancer regulatory genes identified, glyco-oncogenes were enriched (>5% of the identified genes) in ACC, COAD, and PAAD, while glyco-TSGs were enriched in THYM, UCS, PRAD, and UCEC (*SI Appendix*, Fig. S1*H*).

To understand which glycosylation pathways are embedded in the prioritized glyco-oncogenes/TSGs, we analyzed their enrichment in Kyoto encyclopedia of genes and genomes pathways. Among the glyco-oncogenes the enriched pathways included, lysosome biogenesis, GSL biosynthesis (lacto/neolacto and ganglio series), glycosaminoglycan (GAG) biosynthesis (chondroitin sulfate /dermatan sulfate and heparan sulfate/heparin), glycosylphosphatidylinositol (GPI) anchor biosynthesis, other types of O-glycan biosynthesis and mucin type O-glycan biosynthesis (*SI Appendix*, Fig. S1*I*). While glyco-TSGs were enriched in N-glycan biosynthesis, various types of N-glycan biosynthesis, GAG biosynthesis (heparan sulfate/heparin), and GPI anchor biosynthesis (*SI Appendix*, Fig. S1*I*). We analyzed further the GSL biosynthetic pathway since it was the top enriched glycosylation pathway among glyco-oncogenes.

GSL Biosynthetic Pathway Is an Oncogenic Pathway. The genes of the GSL pathway that were classified as potential oncogenes include *B3GNT2, B3GNT3, B3GNT5,* and *FUT4* involved in the biosynthesis of lacto-neolacto series GSLs and *B4GALNT1, ST6GALNAC6,* and *SLC33A1* involved in the biosynthesis of ganglio series GSLs (Fig. 2*A*). In addition, in the list were also present: i) *B4GALT5* encoding for lactosylceramide synthase; ii) *GOLPH3* encoding a recently identified proteostatic regulator of B4GALT5 (9); iii) *ORMDL3* encoding a regulator of sphingolipid biosynthesis (22). Published evidence indicates that many of these genes have oncogenic properties *SI Appendix*, Table S2. We tested whether these genes could drive cellular transformation using the classic NIH3T3 cell assay (hereinafter 3T3 cells). For this, we generated 3T3 cell lines stably transfected with V5 or HA-tagged versions of the GSL pathway oncogenes. We were unable to get stable clones expressing *FUT4* and *SLC33A1,* so they were not included in further analysis. The 3T3 cells showed a stable expression of glycogenes as demonstrated by immunofluorescence analysis, where we also observed that tagged versions of these proteins localized to the Golgi except ORMDL3 and B3GNT5 which had significant ER localization (*SI Appendix*, Fig. S2*A*). To test for the oncogenic property of these cells, we used either anchorage-independent growth assay or cell migration (wound healing) assay. We found that cells expressing the following genes- *B3GNT2, B3GNT3, B4GALT5, B4GALNT1,* and *ST6GALNAC6* showed an increased ability to proliferate and form colonies in anchorage-independent growth assay (Fig. 2 *B* and *C*), while cells expressing *ST6GALNAC6, ORMDL3, B3GNT5,* and *B4GALNT1* showed an increased propensity to migrate in the wound-healing assay (Fig. 2*D*). Finally, to validate if these oncogenes indeed acted through GSL biosynthetic pathway, we selected the cell lines overexpressing B4GALNT1 and B3GNT2 that showed strong effects in anchorage-independent assay and tested their growth in the presence of Miglustat, a well-known inhibitor of GSL production. As shown in Fig. 2*E*, anchorage-independent growth of these cells was inhibited upon Miglustat treatment suggesting that their oncogenic activity is mediated through the GSL biosynthetic pathway. These data indicated that GSL pathway genes identified in our *in-silico* screening indeed are oncogenes and the GSL pathway is a potential oncogenic pathway.

Characterization of B4GALT5 as a Glyco-Oncogene. Next, we sought to better characterize *B4GALT5* for known properties of an oncogene since we recently showed that oncoprotein GOLPH3 promotes oncogenesis through B4GALT5 (9).

B4GALT5 promotes growth in cell lines. We first measured the rate of proliferation of cells expressing *B4GALT5*. 3T3 cells expressing *B4GALT5* proliferated faster compared to control cells as measured by Carboxyfluorescein succinimidyl ester (CFSE) assay (Fig. 3*A*). 3T3 cells expressing *B4GALT5* showed more colonies in soft agar assay compared to empty vector transfected control cells and at levels comparable to that observed following GOLPH3 or RAS^{Val12} overexpression (Fig. 3*B*). In a similar fashion, cells expressing B4GALT5 also showed increased number of foci compared to Green fluorescent protein transfected control cells and again at levels comparable to that observed with cells overexpressing GOLPH3 or RAS^{Val12} mutant (Fig. 3*C*). Further, 3T3 cell lines overexpressing B4GALT5 also showed increased activation of the Akt signaling pathway, a key signaling pathway regulating cell growth and proliferation (Fig. 3*D*). Thus, increased expression of *B4GALT5* confers oncogenic properties including activation of cell growth signaling pathways, increased rate of proliferation, less dependence on anchorage for growth and reduced contact inhibition of growth.

B4GALT5 promotes addiction. The cytoband 20q13.13 containing the *B4GALT5* gene is reported to be frequently amplified in several cancers (23–25). We also find that the *B4GALT5* locus shows significant amplification and a corresponding increase in mRNA levels in six cancer types—BRCA, COAD, ESCA, LIHC, STAD, and UCS. In LIHC, *B4GALT5* gets classified as a Class III glyco-oncogene. Further, increased GSL production has been shown to be essential for hepatocellular carcinoma development (26). So, we first studied the contribution of *B4GALT5* to oncogenesis in hepatocellular carcinoma models.

B4GALT5 expression was silenced in hepatocellular carcinoma cell lines HepG2 (with *B4GALT5* amplification; Fig. 3*E*) and Hep3B cells (diploid for *B4GALT5)* using siRNAs (nontargeting siRNA as control) and their survival was monitored by colony-forming assays. HepG2 showed an increased sensitivity to reduction in B4GALT5 levels compared to Hep3B cells (Fig. 3*F*). We also tested the effects of *B4GALT5-KD* on isogenic 3T3 cell lines with or without stable overexpression of *hB4GALT5*. 3T3 cells stably overexpressing B4GALT5 showed increased sensitivity to reduction in B4GALT5 levels as measured by cell proliferation assay (Fig. 3*G*) and spheroid formation assay (*SI Appendix*, Fig. S2 *B* and *C*). *B4GALT5* is amplified in several cancer types, with ovarian and colon cancers among the prominent ones (*SI Appendix*, Fig. S2*D*). Again, when tested in colony formation assays, ovarian

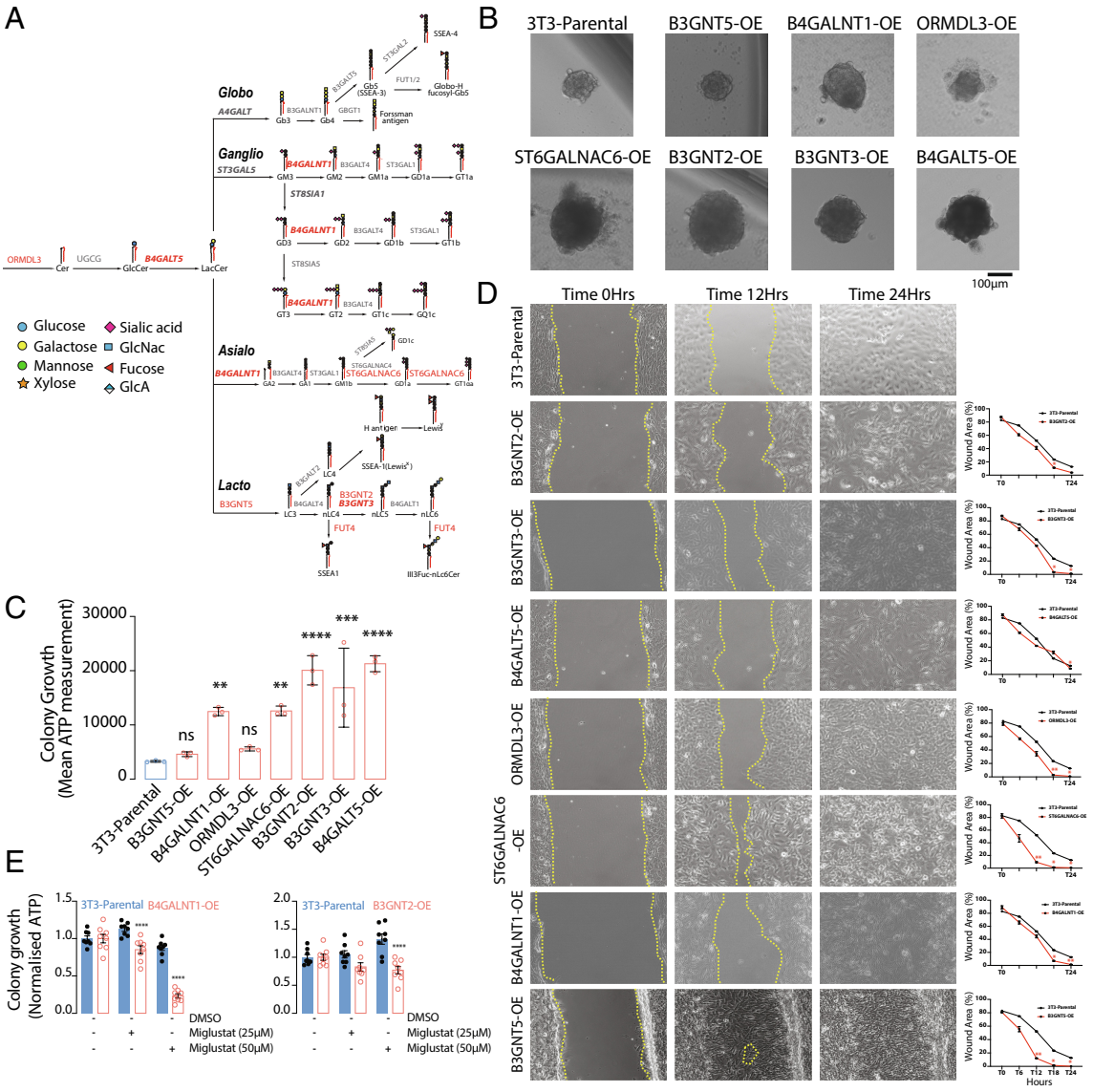

Fig. 2. GSL pathway is an oncogenic pathway. (*A*) Schematic representation of the GSL pathway (in RED are the glycogenes from this study and *BOLD ITALICS* are GOLPH3 clients). (*B*) Representative colony images of glycogene overexpressing 3T3 cells grown in anchorage-independent conditions; (Scale bar, 100 µm.) (*C*) Normalized proliferation of cells overexpressing glycogene compared to parental 3T3 cells as measured using CellTiter-Glo luminescent assay. (*D*) Representative images of cell migration assay (*Left*) and respective quantification (*Right*) from 3T3 cells overexpressing glycogenes compared to parental 3T3 cells. (*E*) Quantification showing the effect on colony growth in B4GALNT1 and B3GNT2 overexpressing 3T3 cells treated with 25 µM and 50 µM of Miglustat. Data show mean ± SEM of three independent experiments: two-tailed Student's *t* test and one-way ANOVA with multiple comparisons. **P* < 0.05, ***P* < 0.01, ****P* < 0.001, and *****P* <0.0001.

and colon cancer cell lines with amplification of *B4GALT5* (*SI Appendix*, Fig. S2*E*) were more sensitive to KD of *B4GALT5* reiterating the earlier findings in hepatocellular carcinoma cell lines (*SI Appendix*, Fig. S2 *F–I*). Thus, cell lines with *B4GALT5* amplification are addicted to B4GALT5 for their increased growth.

Inhibition of B4GALT5 activity reduces cancer cell growth. B4GALT5 transfers galactose onto the glucosylceramide to form lactosylceramide, which serves as the precursor for other complex GSLs. GSLs produced in the cell lines used above were monitored using H^3-Sphingosine pulse–chase (en rule) assay (27). Both B4GALT5 overexpressing 3T3 cells and HepG2 showed high amounts of GSL synthesis compared to parental 3T3 and Hep3B, respectively (*SI Appendix*, Fig. S3 *A* and *B*). Next, we treated HepG2, Hep3B, and 3T3 cell lines with GSL inhibitor Miglustat, and monitored cell proliferation. While Hep3B and 3T3 parental cell lines were nearly insensitive to the treatment, HepG2 cells and B4GALT5 overexpressing 3T3 cells showed a concentration-dependent reduction in cell growth (Fig. 3 *H–J*). Similar inhibitory effects were also observed in colon cell line HCT116 bearing *B4GALT5* amplification, while diploid RKO cell line was insensitive to Miglustat (*SI Appendix*, Fig. S3 *C* and *D*) suggesting that GSL biosynthesis is essential for the growth of cell lines with increased B4GALT5 expression. We then created a catalytically inactive mutant of B4GALT5 by mutating a conserved tryptophan residue, located within the pocket that binds Uridine Diphosphate-Galactose donor (28), to alanine ($B4GALT5^{W296A}$) (*SI Appendix*, Fig. S3*E*). *B4GALT5-KO* HeLa cells (29) analyzed by H^3-Sphingosine pulse chase assay showed lower amounts of complex GSLs and increased precursor lipid, GlcCer compared to control cells (*SI Appendix*, Fig. S3*F*). When expressed in these cells, $B4GALT5^{WT}$ rescued GSL biosynthesis while $B4GALT5^{W296A}$ did not (Fig. 3*K*). Thus, $B4GALT5^{W296A}$ mutant is indeed catalytically inactive. Next, when tested in soft agar assay *B4GALT5-KO* cells formed low number of colonies and expression of $B4GALT5^{WT}$ in these cells increased the number of colonies nearly 10-fold, while expression $B4GALT5^{W296A}$ did not

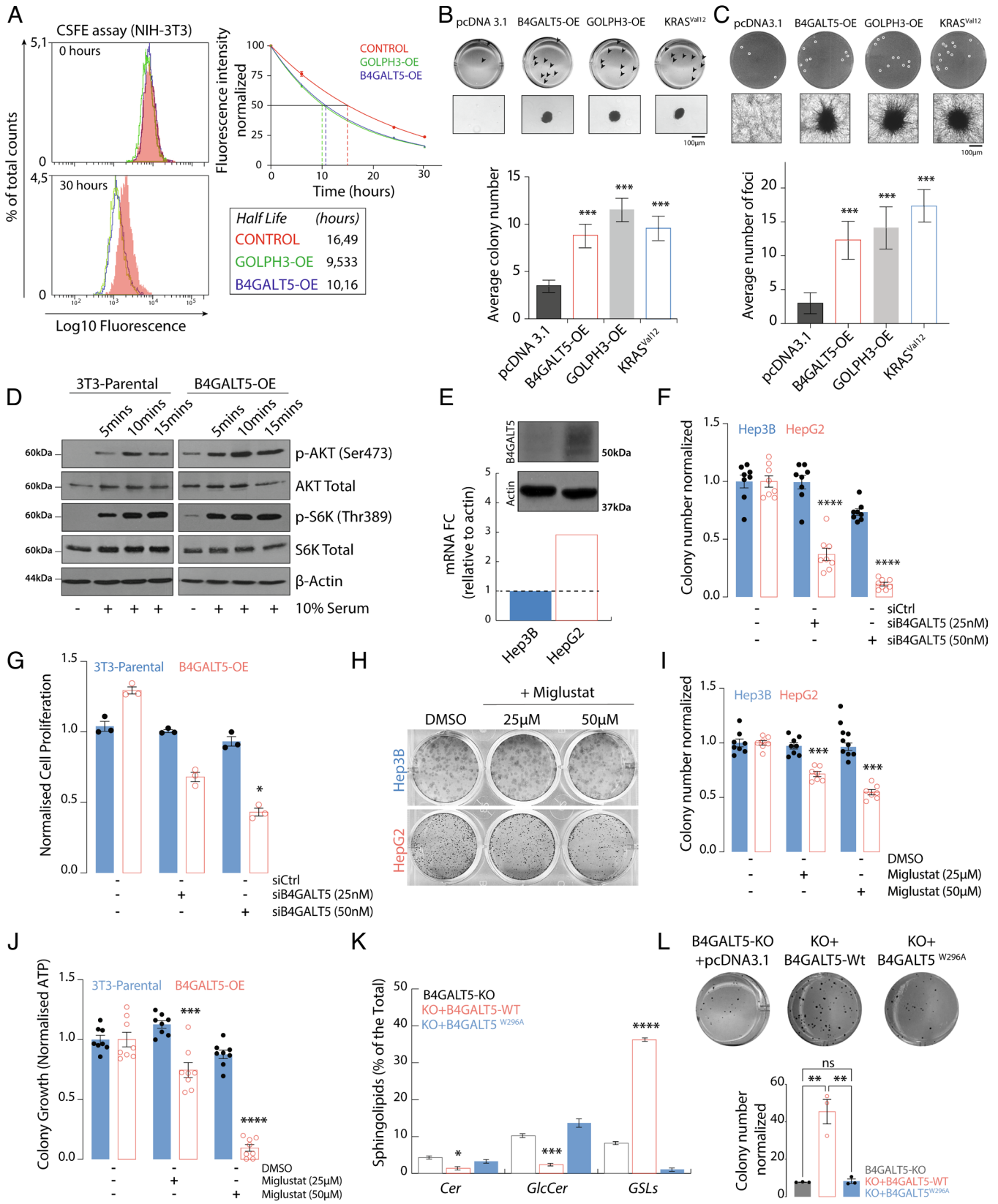

Fig. 3. B4GALT5 promotes oncogenic growth via GSL biosynthesis. (*A*) CFSE proliferation assay in NIH3T3 cells overexpressing B4GALT5 or GOLPH3; histogram (*Left*) and normalized mean fluorescence intensity (*Right*). (*B*) Soft agar and (*C*) foci formation assays in NIH3T3 cells overexpressing B4GALT5 or GOLPH3 with RAS^{Val12}. (*D*) Immunoblots of p-AKT (Ser473) and p-P70S6K (Thr389) in serum-starved B4GALT5-overexpressing cells. (*E*) B4GALT5 protein levels in amplified (red) vs. diploid (blue) liver cancer lines. (*F*) Clonogenic and (*G*) proliferation assays in Hep3B and HepG2 cells treated with *siB4GALT5*. (*H* and *I*) Colony formation in Hep3B and HepG2 cells treated with Miglustat. (*J*) Cell proliferation assay in NIH3T3 cells treated with Miglustat. (*K*) HPTLC sphingolipid analysis [H^3-Sphingosine pulse–chase (en rule)] in *B4GALT5-KO* cells expressing WT or $B4GALT5^{W296A}$ mutant. (*L*) Soft agar images (*Top*) and colony counts (*Bottom*) for *B4GALT5-KO* cells expressing WT or $B4GALT5^{W296A}$ mutant. Data are mean ± SEM (n = 3); two-tailed Student's *t* test. **P* < 0.05, ***P* < 0.01, ****P* < 0.001, and *****P* <0.0001.

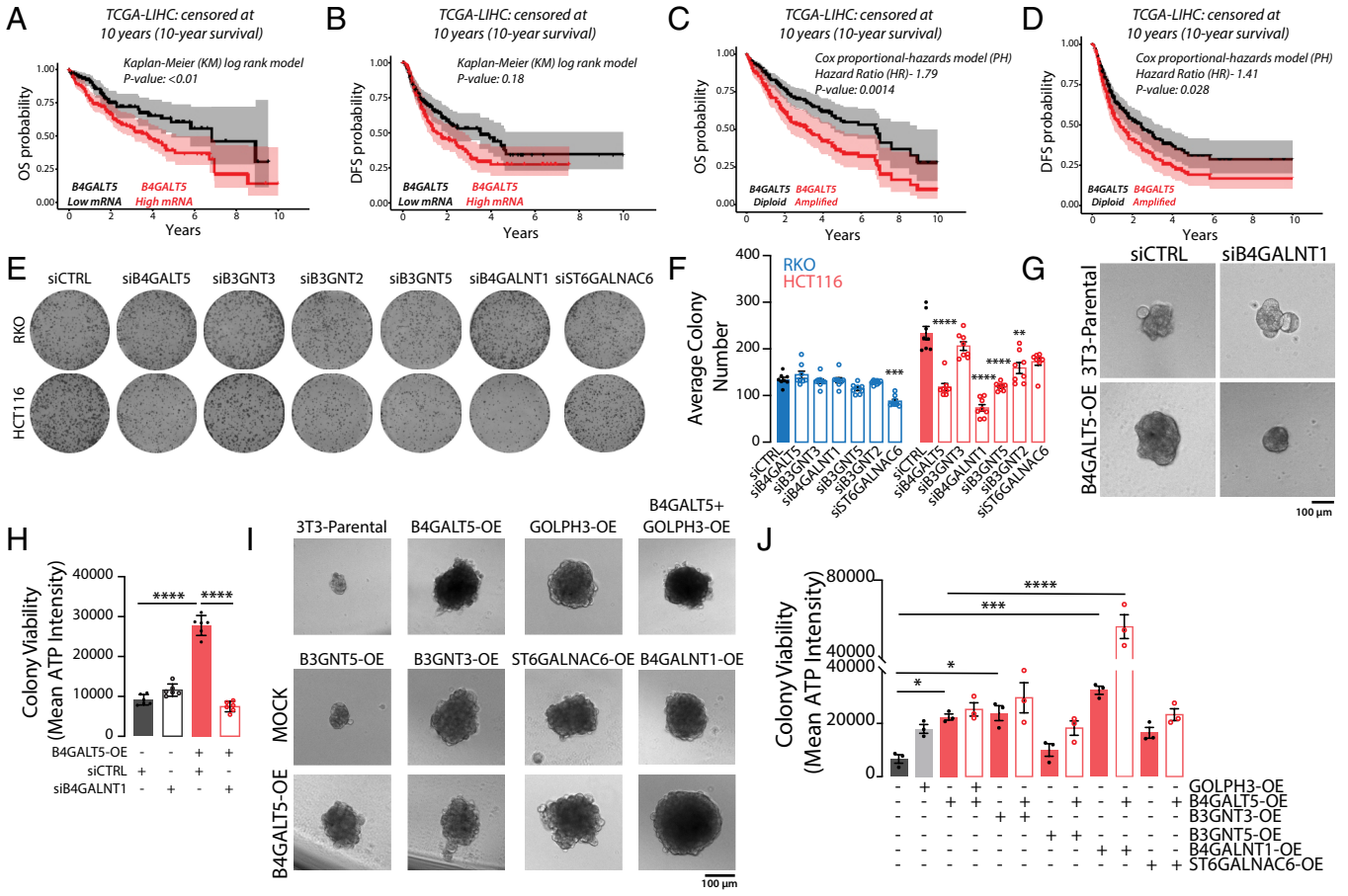

Fig. 4. *B4GALT5* amplification reduces survival and synergizes with *B4GALNT1* to drive oncogenesis. (*A* and *B*) Kaplan-Meier plots of overall and disease-free survival in LIHC patients with high (red) vs. low (black) *B4GALT5* mRNA expression. (*C* and *D*) Cox analysis of overall and disease-free survival in LIHC patients with *B4GALT5* amplification (red) vs. diploid (black) (HR: 1.79 and 1.41, respectively). (*E* and *F*) Clonogenic assay of RKO (diploid; blue) and HCT116 (amplified; red) colon cancer cells treated with indicated siRNAs. (*G* and *H*) Anchorage-independent growth of 3T3-Parental vs. B4GALT5 overexpressing 3T3 cells treated with *siCtrl* or *siB4GALNT1*; (Scale bar, 100 µm.) (*I* and *J*) Anchorage-independent growth and viability of 3T3 cells overexpressing glyco-oncogenes alone or with B4GALT5; (Scale bar, 100 µm.) Data are mean ± SEM (n = 3), one-way ANOVA with Tukey's multiple comparison test. *P < 0.05, **P < 0.01, ***P < 0.001, and ****P <0.0001.

show a change in the number of colonies (Fig. 3*L*). Collectively, these findings suggest that enzymatic activity of B4GALT5 was required for its oncogenic property.

Increased B4GALT5 expression worsens patient survival. We next compared the survival in cancer patients who displayed high *B4GALT5* expression with those who did not. LIHC patients with increased expression of *B4GALT5* showed a worse overall survival and disease-free survival compared to those with no *B4GALT5* upregulation (Fig. 4 *A* and *B*). Similar results were also demonstrated by others using other cancer-specific cohorts (30). Furthermore, LIHC patients with high levels of *B4GALT5* amplification showed a reduced overall survival (Fig. 4 *C* and *D*). This suggests that the *B4GALT5*-induced oncogenic aggressiveness has a potential impact on the clinical outcome.

From these studies, we observed *B4GALT5* amplification results in increased levels of its activity and product, which contributes to oncogenic properties in both laboratory studies (promotion of anchorage-independent growth, oncogenic addiction) and clinical evaluation (worsened survival). Thus, *B4GALT5* demonstrates all key features that define an oncogene.

B4GALT5 Acts Mainly Through the Ganglioside Biosynthetic Pathway. B4GALT5 lies at a branch point in the GSL biosynthetic pathway leading to ganglioside and lacto/neolacto GSL synthesis, both enriched among glyco-oncogenes. To identify which pathway acts downstream, colon cancer cell lines RKO (*B4GALT5* diploid) and HCT116 (*B4GALT5* amplified) were treated with siRNAs targeting pathway enzymes, and growth was assessed by colony formation. Targets included *B3GNT2, B3GNT3, B3GNT5, B4GALNT1,* and *ST6GALNAC6*, with knockdown confirmed by qPCR (*SI Appendix*, Fig. S3*G*). B4GALNT1 and ST6GALNAC6 function in ganglioside synthesis, others in lacto/neolacto synthesis. *ST6GALNAC6* knockdown showed modest effect in both lines (Fig. 4 *E* and *F*), indicating B4GALT5-independent effects. In contrast, *B4GALNT1* knockdown strongly inhibited HCT116 growth (Fig. 4 *E* and *F*), suggesting B4GALT5 acts mainly through ganglioside synthesis leading to GD2. Of note, GD2 has earlier been implicated in carcinogenesis (31, 32). Lacto/neolacto enzymes also affected growth, especially B3GNT5, but less than B4GALNT1 (Fig. 4 *E* and *F*). Thus, B4GALT5 influences both pathways, with ganglioside GD2 likely providing the dominant growth contribution. This was validated in 3T3 cells overexpressing B4GALT5: Parental cells were insensitive to *B4GALNT1* knockdown, whereas B4GALT5-overexpressing cells were strongly inhibited (Fig. 4 *G* and *H*), thus confirming action through ganglioside biosynthesis.

We next tested whether B4GALT5 synergizes with other GSL enzymes in 3T3 cells. As expected, coexpression with GOLPH3 showed no synergy (Fig. 4 *I* and *J* and *SI Appendix*, Fig. S3 *H* and *I*), since both act at the same step. Strong additivity was observed

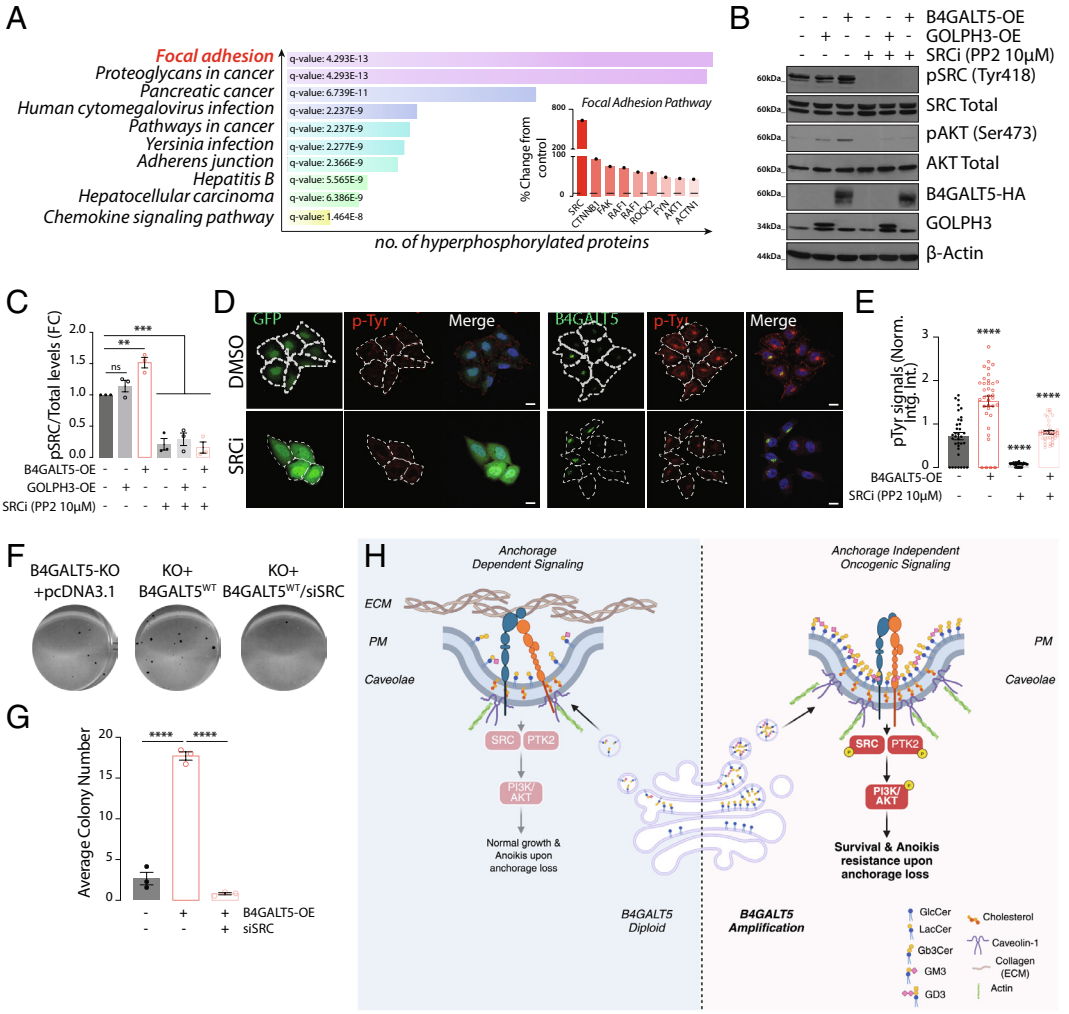

Fig. 5. B4GALT5 activates Src kinase and promotes survival and growth upon adherence loss. (*A*) Gene ontology enrichment of hyperphosphorylated proteins in B4GALT5^{WT} overexpression vs. *B4GALT5-KO* HeLa cells; phosphorylation of the focal adhesion pathway (*Top* hits) is plotted as percent change from control. (*B* and *C*) Immunoblot and quantification of Src activation in B4GALT5^{WT} overexpressing *B4GALT5-KO* cells; PP2 (Src inhibitor) served as a control. (*D* and *E*) Immunofluorescence and quantification of p-Tyr signals in B4GALT5^{WT} overexpressing cells. (*F* and *G*) Soft agar colony images and counts for B4GALT5^{WT} expressing *B4GALT5-KO* cells with or without *siSRC*. (*H*) Schematic model of B4GALT5-mediated onco-GSL levels and adherence-independent growth; increased GSLs in amplified tumors enhance integrin clustering to activate Src/FAK and the downstream PI3K/Akt/mTOR pathway. Data are mean ± SEM (n = 3); one-way ANOVA with Tukey's multiple comparisons. *P < 0.05, **P < 0.01, ***P < 0.001, and ****P <0.0001.

between B4GALT5 and B4GALNT1 (Fig. 4 *I* and *J*), consistent with their roles at different steps of the same pathway. Knocking down B3GNT5 and ST6GALNAC6 had modest individual effects and did not enhance B4GALT5-driven growth (Fig. 4 *I* and *J*). B3GNT3 alone promoted growth similarly to B4GALT5, but coexpression showed no additivity despite acting at different pathway levels (Fig. 4 *I* and *J*), possibly due to shared effects on ceramide reduction rather than complex GSL production. Overall, these findings indicate that B4GALT5 primarily promotes cell growth through the ganglioside biosynthetic pathway.

B4GALT5 Activates the Integrin-Src Signaling Pathway to Promote Anchorage-independent Growth. Next, we analyzed signaling pathways modulated by B4GALT5 overexpression using a phosphoproteomic antibody microarray. *B4GALT5-KO* HeLa cells were transfected with B4GALT5^{WT} and assessed for phosphorylation changes under suspension conditions mimicking detachment. The most prominent alterations centered on integrin signaling (Fig. 5*A*), a key mediator of anoikis resistance (33). Src phosphorylation at Tyr418 was strongly increased (Fig. 5*A* and Dataset S5), along with FAK, CTNNB1, RAF1, ROCK2, FYN, ACTN1, and AKT1—core components of focal adhesion survival pathways (Fig. 5*A*). These experiments were performed in suspension, where loss of integrin-ECM engagement typically suppresses signaling and induces apoptosis. However, B4GALT5-expressing cells retained integrin-Src activation, suggesting restoration of signaling in detachment.

Western blotting confirmed increased phospho-Src (Tyr418), which was abolished by the Src inhibitor PP2 (Fig. 5 *B* and *C*). Immunofluorescence showed elevated phospho-tyrosine staining, again suppressed by PP2 (Fig. 5 *D* and *E*). Src normally activates PI3K/Akt and Ras/Raf pathways downstream of integrin engagement. Consistently, phospho-Akt (Ser473) and phospho-S6 kinase (Thr389) were elevated in B4GALT5-overexpressing cells (Fig. 5*B* and *SI Appendix*, Fig. S4*A*), and PP2 reduced both phospho-Src and phospho-Akt, indicating Src-dependent activation. Src activation required B4GALT5 catalytic activity, as the inactive B4GALT5^{W296A} mutant failed to elevate phospho-tyrosine signals (*SI Appendix*, Fig. S4 *B*–*D*). Functionally, Src was essential as knockdown of *SRC* abolished B4GALT5-driven anchorage-independent growth in soft agar (Fig. 5 *F* and *G*). Together, these results show that B4GALT5 maintains integrin-Src signaling in the absence of adhesion, preventing anoikis.

Based on the role of GSLs in integrin signaling, we propose that elevated GSLs in B4GALT5-overexpressing cells promote glycolipid-enriched membrane domains, facilitating integrin clustering and activation (Fig. 5*H*) (34, 35). This activates Src and Akt pathways (*SI Appendix*, Fig. S4 *E* and *F*), supporting adhesion-independent survival and growth.

Discussion

Oncogenes and TSGs arise from normal protogenes that acquire genetic alterations leading to constitutive changes in protein activity and downstream signaling that drive tumor growth (36). These three features- genetic alteration, altered product activity, and signaling rewiring- together define a cancer regulatory gene and create therapeutically relevant dependencies. This study demonstrates all three characteristics among genes in the GSL biosynthetic pathway, consolidating their role in cancer development (37, 38) and identifying a new class of enzymatic drug targets.

The identified glyco-oncogenes were enriched in lacto/neolacto and ganglio-series GSL biosynthesis and O-glycan biosynthesis, whereas glyco-TSGs were enriched in N-glycan biosynthesis. The O-glycan group mainly involved O-mannosylation enzymes linked to oncogenesis via NOTCH signaling (39, 40). In contrast, the tumor-suppressive association of N-glycan genes-largely early secretory pathway enzymes (Endoplasmic Reticulum and *cis*-Golgi) was unexpected. Although N-glycan branching is often linked to tumor promotion, several observations support a TSG role for early N-glycosylation: increased pausimannose in tumors (41), its association with aggressive gastric cancer (42), and oncogenic effects of metabolic stress from impaired N-glycan biosynthesis (43). Additionally, TUSC3 has been proposed as a tumor suppressor (44), supporting our conclusions.

We previously showed that the oncogene GOLPH3 stabilizes B4GALT5 (9); here we show that *B4GALT5* itself functions as an oncogene. It promotes growth in glioma, breast, and hepatocellular cancers and is a potential colorectal cancer target (30, 45–48). Its oncogenicity depends on catalytic activity and operates in hepatocellular, colorectal, and ovarian cancers. B4GALT5 increases complex GSLs while reducing ceramide (9), and our data suggest GD2 may act downstream. Notably, B3GNT3 and B4GALT5 act at the same level in progrowth signaling despite different pathway positions, likely through shared effects on ceramide consumption.

A key finding here is that B4GALT5 overexpression preserves integrin-mediated signaling under nonadherent conditions, preventing anoikis. Sustained Src activation and phospho-tyrosine signaling in suspension enable anchorage-independent survival, a critical step in metastatic dissemination (33).

GSLs support tumor growth by enhancing lipid raft formation and by acting as bioactive ligands for receptors such as c-Met, epidermal growth factor receptor, and integrins (38, 49–51). Increased GSLs likely promote membrane domains that cluster and activate integrins without matrix attachment, sustaining Src and downstream PI3K/Akt/mTOR survival pathways (52, 53). Src inhibition abolishes B4GALT5-driven growth in suspension, identifying it as a key effector. Thus, B4GALT5-mediated integrin-Src signaling provides a mechanism of anoikis resistance that may enhance metastatic potential. Further work should define the integrin subtypes involved and test whether targeting B4GALT5 or Src impairs metastatic colonization in vivo.

Materials and Methods

Cell Lines and Culture Conditions. See *SI Appendix* for details and *SI Appendix*, Table S3.

Stable Cell Line Generation. 3T3 cells were either transfected with pLX304 plasmids (kind gift from Giovanni D'Angelo, EPFL Switzerland) or transduced with lentivirus particles with polybrene (2.5 μg/mL) at a suboptimal confluency for 24 h followed by antibiotic (20 μM blasticidin) selection. Resistant clones were thereafter maintained in DMEM containing 5% fetal bovine serum (FBS), 2 mM L-Glutamine, and 100U/ml penicillin and streptomycin. Overexpression of the respective glycogene was confirmed by either V5- or HA-tag expression by immunofluorescence. All the plasmid vectors are enlisted in *SI Appendix*, Table S4.

Transfection and RNAi. DNA transfection was done with either MIRUS or Lipofectamine LTX and siRNAs were transfected using Oligofectamine as per the manufacturer's instructions. For a list of siRNAs, see *SI Appendix*, Table S5.

Functional Assays. *Anchorage-independent growth:* $1X10^4$ cells were suspended in 0.3% agarose over a 0.6% agarose base and incubated for 30 d under physiological conditions.

Clonogenic and Foci Formation: For clonogenic assays, siRNA-transfected cells (100/well) were grown in low serum for 14 d. For foci formation, plasmid-transfected cells were maintained at high confluency in 2.5% serum for 15 to 20 d. All colonies/foci were fixed, stained with 0.1% crystal violet, and quantified via ImageJ.

3D Spheroids: Cells (1000/well) were seeded in ultralow attachment U-bottom plates. Spheroids were treated with drugs for 15 d, imaged using Opera Phenix, and analyzed with Harmony software.

Migration assay: Cells were plated optimally to attain high confluency the following day. A scratch at the center of each well was made using a sterile microtip. Images at 20X magnification were acquired every 6 h using Zeiss Apotome III microscope. Quantification was performed using the ImageJ plugin.

Flow Cytometry Analysis. *CFSE proliferation assay:* Cells were labeled with CFSE dye for 10 min at 37 °C, quenched with complete media, and plated at 50,000 cells/well. Following overnight incubation, proliferation was analyzed using a FACS ARIA III cell sorter.

Immunoblotting and Phosphoproteomics. Cells were washed twice with PBS and lysed in RIPA buffer (150 mM NaCl, 1% Triton X-100, 0.5% deoxycholic acid, 0.1% SDS, and 20 mM Tris-HCl, pH 7.4), supplemented with protease and phosphatase cocktail inhibitor (Roche). For signaling experiments, cells were serum starved overnight and stimulated with 10% serum at different time points before lysing. The lysates were clarified by centrifugation at high rpm for 5 min and quantified using a BCA Protein Assay kit (Pierce). Proteins were resolved on a 12% denaturing polyacrylamide gel and immunoblotted with respective primary antibodies followed by second antibodies conjugated with HRP and then developed using the chemiluminescence kit (Pierce).

To assess the global phosphorylation changes, cells were maintained in 1% FBS containing media overnight. Cells were harvested by trypsinization, washed twice with cold PBS, and cell pellets were shipped to Kinexus (KAM-1300P; System proteomic company, Vancouver, Canada). Changes ≥ 50% Changes from control and Z ratio ≥ +1.00 (hyperphosphorylation) or ≤ −1.00 (dephosphorylation) were considered as real significant changes.

Immunofluorescence. Cells were fixed in 4% paraformaldehyde, permeabilized with 0.2% saponin, and incubated with primary antibodies (*SI Appendix*, Table S6) followed by Alexa Fluor-conjugated secondaries. Coverslips were mounted with Mowiol/Glycerol containing Hoechst and imaged using confocal microscopy (LSM980, Carl Zeiss).

3H-Sphingosine Pulse–Chase (en rule) and HPTLC. Briefly, cells were pulse-labeled with 0.1 μCi/ml (~5 nM) 3H-D-erythro-Sphingosine for 2 h and chased for 24 h. Subsequently, cells were harvested and lipids extracted using an extraction buffer (200 μL of 200 mM KCL, 500 μL methanol, 250 μL chloroform, and 250 μL KCL). Finally, lipids were spotted on silica gel high performance–TLC plates (Merck, Germany) and resolved using a mixture of chloroform: methanol: water (65: 25: 4 v/v/v) in a closed glass chamber. After separation, radiolabeled lipids were analyzed using a RITA TLC Analyzer (Raytest, Germany) and quantified using GINA (Raytest, Germany) software.

Real-Time qPCR and mRNA Analysis. Total RNA was isolated (Rneasy kit, Qiagen), reverse transcribed, and analyzed via qPCR using SYBR Green on a LightCycler® 480 II detection system (Roche). Expression was calculated using the ΔΔCt method normalized to HPRT1 (*SI Appendix*, Table S5).

Statistical Analyses. Graph values are expressed as mean ±SEM of at least three independent biological replicates and normalized to respective controls. The nonparametric test was applied to data which did not follow normal distribution. Test statistics were performed using GraphPad Prism 10, and *P*-values were determined either by Student's *t* test or multiple comparisons using one-way ANOVA (Türkiye's test).

Data, Materials, and Software Availability. Bioinformatics Pipeline data have been deposited in Github (31). All study data are included in the article and/or supporting information.

ACKNOWLEDGMENTS. We thank Dr. Luigi Concilio for plasmid purification. P.S. acknowledges Dr. Marialuisa Moccia from FC lab and Dr. Marianna Matarese for assisting in stable cell line generation and Dr. Marinella Pirozzi for microscopy assistance. We thank the Euro Bioimaging facility for the access to the microscopes. S.P. acknowledges financial support from Ministry of University and Research (MUR) (PRIN2022PNRR-2022MZJR9X, P2022YA3LL). D.R. acknowledges financial support from MUR (PRIN2022PNRR P2022MMPXH) and MUR Piano Nazionale di Ripresa e Resilienza) (PNRR) "National Center for Gene Therapy and Drugs based on RNA Technology" (Project no. CN00000041 CN3 RNA). A.L. acknowledges financial support from the Associazione Italiana per la Ricerca sul Cancro (Projects IG 15767 and IG 20786), TERABIO, PON\IMPARA, and S.A.T.I.N. P.S. was supported by the PNRR project SEE LIFE–StrEngthEning the ItaLIan InFrastructure of Euro-bioimaging," code: "IR0000023"–CUP B53C22001810006.

Author affiliations: [a]Institute of Endotypes in Oncology, Metabolism and Immunology "G. Salvatore," National Research Council of Italy, Naples 80131, Italy; [b]Institute of Nanotechnology, National Research Council of Italy, Leece 73100, Italy; [c]Cell Biology and Biotherapy Unit, Istituto Nazionale Tumori–Istituto di Ricovero e Cura a Carattere Scientifico–"Fondazione G. Pascale", Napoli 80131, Italy; [d]Unit of Cellular Networks and Molecular Therapeutic Targets, Istituto di Ricovero e Cura a Carattere Scientifico Regina Elena National Cancer Institute, Rome I-00144, Italy; and [e]Dipartimento di Medicina Molecolare e Biotecnologie Mediche, Università Di Napoli "Federico II", Naples 80131, Italy

1. S. S. Pinho, C. A. Reis, Glycosylation in cancer: Mechanisms and clinical implications. *Nat. Rev. Cancer* **15**, 540–555 (2015).
2. S. R. Stowell, T. Ju, R. D. Cummings, Protein glycosylation in cancer. *Annu. Rev. Pathol. Mech. Dis.* **10**, 473–510 (2015).
3. C. Cumin *et al.*, Glycosphingolipids are mediators of cancer plasticity through independent signaling pathways. *Cell Rep.* **40**, 111181 (2022).
4. D. M. Hercules, Chemiluminescence resulting from electrochemically generated species. *Science* **145**, 808–809 (1964).
5. K. Santhanam, A. J. Bard, Chemiluminescence of electrogenerated 9, 10-diphenylanthracene anion radical1. *J. Am. Chem. Soc.* **87**, 139–140 (1965).
6. B. Vogelstein *et al.*, Cancer genome landscapes. *Science* **339**, 1546–1558 (2013).
7. K. L. Scott *et al.*, GOLPH3 modulates mTOR signalling and rapamycin sensitivity in cancer. *Nature* **459**, 1085–1090 (2009).
8. H. C. Dippold *et al.*, *GOLPH3* bridges phosphatidylinositol–4–phosphate and actomyosin to stretch and shape the Golgi to promote budding. *Cell* **139**, 337–351 (2009).
9. R. Rizzo *et al.*, Golgi maturation-dependent glycoenzyme recycling controls glycosphingolipid biosynthesis and cell growth via GOLPH3. *EMBO J.* **40**, e107238 (2021).
10. T. Isaji *et al.*, An oncogenic protein Golgi phosphoprotein 3 up-regulates cell migration via sialylation. *J. Biol. Chem.* **289**, 20694–20705 (2014).
11. E. S. Eckert *et al.*, Golgi phosphoprotein 3 triggers signal-mediated incorporation of glycosyltransferases into coatomer-coated (COPI) vesicles. *J. Biol. Chem.* **289**, 31319–31329 (2014).
12. J. D. Thomas *et al.*, Rab1A is an mTORC1 activator and a colorectal oncogene. *Cancer Cell* **26**, 754–769 (2014).
13. N. Halberg *et al.*, PITPNC1 recruits RAB1B to the Golgi network to drive malignant secretion. *Cancer Cell* **29**, 339–353 (2016).
14. X. Tan *et al.*, PI4KIIIβ is a therapeutic target in chromosome 1q–amplified lung adenocarcinoma. *Sci. Transl. Med.* **12**, eaax3772 (2020).
15. T. Santarius, J. Shipley, D. Brewer, M. R. Stratton, C. S. Cooper, A census of amplified and overexpressed human cancer genes. *Nat. Rev. Cancer* **10**, 59–64 (2010).
16. J. Gao *et al.*, Integrative analysis of complex cancer genomics and clinical profiles using the cBioPortal. *Sci. Signal.* **6**, pl1 (2013).
17. C. H. Mermel *et al.*, 0 facilitates sensitive and confident localization of the targets of focal somatic copy-number alteration in human cancers. *Genome Biol.* **12**, 1–14 (2011).
18. M. Bouhaddou *et al.*, Mapping the protein–protein and genetic interactions of cancer to guide precision medicine. *Curr. Opin. Genet. Dev.* **54**, 110–117 (2019).
19. R. Beroukhim *et al.*, The landscape of somatic copy-number alteration across human cancers. *Nature* **463**, 899–905 (2010).
20. D. Škalamera *et al.*, A high-throughput platform for lentiviral overexpression screening of the human ORFeome. *PLoS One* **6**, e20057 (2011).
21. J. Nulsen, H. Misetic, C. Yau, F. D. Ciccarelli, Pan-cancer detection of driver genes at the single-patient resolution. *Genome Med.* **13**, 1–14 (2021).
22. D. K. Breslow *et al.*, Orm family proteins mediate sphingolipid homeostasis. *Nature* **463**, 1048–1053 (2010).
23. J. G. Hodgson, K. Chin, C. Collins, J. W. Gray, Genome amplification of chromosome 20 in breast cancer. *Breast Cancer Res. Treat.* **78**, 337–345 (2003).
24. D. Wang *et al.*, Multiple genes identified as targets for 20q13. 12–13.33 gain contributing to unfavorable clinical outcomes in patients with hepatocellular carcinoma. *Hepatol. Int.* **9**, 438–446 (2015).
25. R. N. Ptashkin *et al.*, Chromosome 20q amplification defines a subtype of microsatellite stable, left-sided colon cancers with wild-type RAS/RAF and better overall survival. *Mol. Cancer Res.* **15**, 708–713 (2017).
26. R. Jennemann *et al.*, Inhibition of hepatocellular carcinoma growth by blockade of glycosphingolipid synthesis. *Oncotarget* **8**, 109201 (2017).
27. D. Russo *et al.*, Glycosphingolipid metabolic reprogramming drives neural differentiation. *EMBO J.* **37**, e97674 (2018).
28. B. Ramakrishnan, P. K. Qasba, Crystal structure of lactose synthase reveals a large conformational change in its catalytic component, the β1, 4-galactosyltransferase-I. *J. Mol. Biol.* **310**, 205–218 (2001).
29. T. Yamaji, K. Hanada, Establishment of HeLa cell mutants deficient in sphingolipid-related genes using TALENs. *PLoS One* **9**, e88124 (2014).
30. Y. Han *et al.*, B4Galt5 high expression associated with poor prognosis of hepatocellular carcinoma. *BMC Cancer* **22**, 392 (2022).
31. F. Russo, Prioritization of driver genes based on CNA (dataset). GitHub. https://github.com/franruss/Prioritization-of-driver-genes-based-on-CNA. Accessed 6 May 2025.
32. H. Yoshida *et al.*, B4GALNT1 induces angiogenesis, anchorage independence growth and motility, and promotes tumorigenesis in melanoma by induction of ganglioside GM2/GD2. *Sci. Rep.* **10**, 1199 (2020).
33. M. L. Taddei, E. Giannoni, T. Fiaschi, P. Chiarugi, Anoikis: An emerging hallmark in health and diseases. *J. Pathol.* **226**, 380–393 (2012).
34. Y. Ohkawa *et al.*, Ganglioside GD3 enhances adhesion signals and augments malignant properties of melanoma cells by recruiting integrins to glycolipid-enriched microdomains. *J. Biol. Chem.* **285**, 27213–27223 (2010).
35. R. Wang *et al.*, Sulfatide interacts with and activates integrin αVβ3 in human hepatocellular carcinoma cells. *Oncotarget* **7**, 36563 (2016).
36. D. Hanahan, R. A. Weinberg, Hallmarks of cancer: The next generation. *Cell* **144**, 646–674 (2011).
37. X. Huang *et al.*, Ganglioside GM3 inhibits hepatoma cell motility via down-regulating activity of EGFR and PI3K/AKT signaling pathway. *J. Cell. Biochem.* **114**, 1616–1624 (2013).
38. A. Cazet *et al.*, The ganglioside GD2 induces the constitutive activation of c-Met in MDA-MB-231 breast cancer cells expressing the GD3 synthase. *Glycobiology* **22**, 806–816 (2012).
39. P. Stanley, T. Okajima, Roles of glycosylation in notch signaling. *Curr. Top. Dev. Biol.* **92**, 131–164 (2010).
40. N. A. Rana, R. S. Haltiwanger, Fringe benefits: Functional and structural impacts of O-glycosylation on the extracellular domain of notch receptors. *Curr. Opin. Struct. Biol.* **21**, 583–589 (2011).
41. S. Chatterjee *et al.*, Protein paucimannosylation is an enriched N-glycosylation signature of human cancers. *Proteomics* **19**, 1900010 (2019).
42. D. Ferreira *et al.*, Trimmed n-glycans define aggressive gastric cancer and predict clinical outcomes. *Theranostics* **15**, 9375–9398 (2025).
43. S. Iwamoto *et al.*, Tolerable glycometabolic stress boosts cancer cell resilience through altered N-glycosylation and notch signaling activation. *Cell Death Dis.* **15**, 53 (2024).
44. P. Horak *et al.*, TUSC3 loss alters the ER stress response and accelerates prostate cancer growth in vivo. *Sci. Rep.* **4**, 3739 (2014).
45. Y. Wei *et al.*, B1, 4-galactosyltransferase V regulates self-renewal of glioma-initiating cell. *Biochem. Biophys. Res. Commun.* **396**, 602–607 (2010).
46. J. Jiang *et al.*, β1, 4-galactosyltransferase V functions as a positive growth regulator in glioma. *J. Biol. Chem.* **281**, 9482–9489 (2006).
47. W. Tang, M. Li, X. Qi, J. Li, B1, 4-galactosyltransferase V modulates breast cancer stem cells through Wnt/β-catenin signaling pathway. *Cancer Res. Treat.* **52**, 1084–1102 (2020).
48. S. B. Chatterjee *et al.*, Lactosylceramide synthase β-1, 4-GalT-V: A novel target for the diagnosis and therapy of human colorectal cancer. *Biochem. Biophys. Res. Commun.* **508**, 380–386 (2019).
49. D. Lingwood, K. Simons, Lipid rafts as a membrane-organizing principle. *Science* **327**, 46–50 (2010).
50. K. Simons, D. Toomre, Lipid rafts and signal transduction. *Nat. Rev. Mol. Cell Biol.* **1**, 31–39 (2000).
51. A. R. Todeschini, S.-I. Hakomori, Functional role of glycosphingolipids and gangliosides in control of cell adhesion, motility, and growth, through glycosynaptic microdomains. *Biochim. Biophys. Acta* **1780**, 421–433 (2008).
52. Z. Sun, S. S. Guo, R. Fässler, Integrin-mediated mechanotransduction. *J. Cell Biol.* **215**, 445–456 (2016).
53. Z. Deng, H. Wang, J. Liu, Y. Deng, N. Zhang, Comprehensive understanding of anchorage-independent survival and its implication in cancer metastasis. *Cell Death Dis.* **12**, 629 (2021).